Clinical Cancer Research

Targeting the MYCN–PARP–DNA Damage Response Pathway in Neuroendocrine Prostate Cancer

Wei Zhang[1,2], Bo Liu[1,3], Wenhui Wu[4], Likun Li[1], Bradley M. Broom[4], Spyridon P. Basourakos[1], Dimitrios Korentzelos[1], Yang Luan[1,5], Jianxiang Wang[1], Guang Yang[1], Sanghee Park[1], Abul Kalam Azad[1], Xuhong Cao[6], Jeri Kim[1], Paul G. Corn[1], Christopher J. Logothetis[1], Ana M. Aparicio[1], Arul M. Chinnaiyan[6], Nora Navone[1], Patricia Troncoso[7], and Timothy C. Thompson[1]

Abstract

Purpose: We investigated MYCN-regulated molecular pathways in castration-resistant prostate cancer (CRPC) classified by morphologic criteria as adenocarcinoma or neuroendocrine to extend the molecular phenotype, establish driver pathways, and identify novel approaches to combination therapy for neuroendocrine prostate cancer (NEPC).

Experimental Design and Results: Using comparative bioinformatics analyses of CRPC-Adeno and CRPC-Neuro RNA sequence data from public data sets and a panel of 28 PDX models, we identified a MYCN–PARP–DNA damage response (DDR) pathway that is enriched in CRPC with neuroendocrine differentiation (NED) and CRPC-Neuro. ChIP-PCR assay revealed that N-MYC transcriptionally activates PARP1, PARP2, BRCA1, RMI2, and TOPBP1 through binding to the promoters of these genes. MYCN or PARP1 gene knockdown significantly reduced the expression of MYCN–PARP–DDR pathway genes and NED markers, and inhibition with MYCNsi and/or PARPsi, BRCA1si, or RMI2si significantly suppressed malignant activities, including cell viability, colony formation, and cell migration, in C4-2b4 and NCI-H660 cells. Targeting this pathway with AURKA inhibitor PHA739358 and PARP inhibitor olaparib generated therapeutic effects similar to those of gene knockdown *in vitro* and significantly suppressed tumor growth in both C4-2b4 and MDACC PDX144-13C subcutaneous models *in vivo*.

Conclusions: Our results identify a novel MYCN–PARP–DDR pathway that is driven by N-MYC in a subset of CRPC-Adeno and in NEPC. Targeting this pathway using *in vitro* and *in vivo* CRPC-Adeno and CRPC-Neuro models demonstrated a novel therapeutic strategy for NEPC. Further investigation of N-MYC–regulated DDR gene targets and the biological and clinical significance of MYCN–PARP–DDR signaling will more fully elucidate the importance of the MYCN–PARP–DDR signaling pathway in the development and maintenance of NEPC.
Clin Cancer Res; 24(3); 696–707. ©2017 AACR.

Introduction

Metastatic castration-resistant prostate cancer (mCRPC), which progresses and metastasizes after surgical or medical castration, is the most common cause for prostate cancer–related deaths (1). The vast majority of mCRPCs arise from prostate cancers that display adenocarcinoma morphology but a subset display small cell or poorly differentiated neuroendocrine prostate cancer (NEPC; ref. 2). NEPC is present in less than 2% of primary localized prostate cancer but often emerges during progression of the disease and is more prevalent in the castration-resistant setting (2–4). The disease associated with NEPC morphology and differentiation has a virulent behavior and poor response to existing therapies and, as a result, most patients with aggressive NEPC succumb to the disease within a year (5). A major hurdle in the diagnosis and treatment of lethal prostate cancer is lack of understanding of the molecular mechanisms that underlie the development of NEPC.

The phenotypic conversion to NEPC has been associated with specific genetic lesions including overexpression and gene amplification of *MYCN* (encoding N-MYC oncoprotein) and *AURKA* (encoding Aurora kinase A, which stabilizes N-MYC; ref. 4). *MYCN*

[1]Department of Genitourinary Medical Oncology, The University of Texas MD Anderson Cancer Center, Houston, Texas. [2]Department of Urology, Changhai Hospital, Second Military Medical University, Shanghai, China. [3]Department of Oncology, Tongji Hospital, Tongji Medical College, Huazhong University of Science and Technology, Wuhan, Hubei, China. [4]Department of Bioinformatics and Computational Biology, The University of Texas MD Anderson Cancer Center, Houston, Texas. [5]Department of Urology, Tongji Hospital, Tongji Medical College, Huazhong University of Science and Technology, Wuhan, Hubei, China. [6]Michigan Center for Translational Pathology, Howard Hughes Medical Institute, Comprehensive Cancer Center, University of Michigan Medical School, Ann Arbor, Michigan. [7]Department of Pathology, The University of Texas MD Anderson Cancer Center, Houston, Texas.

Note: Supplementary data for this article are available at Clinical Cancer Research Online (http://clincancerres.aacrjournals.org/).

W. Zhang and B. Liu contributed equally to this article.

Corresponding Author: Timothy C. Thompson, Department of Genitourinary Medical Oncology, The University of Texas MD Anderson Cancer Center, 1515 Holcombe Boulevard, Unit 18-3, Houston, TX 77030. Phone: 713-792-9955; Fax: 713-792-9956; E-mail: timthomp@mdanderson.org

doi: 10.1158/1078-0432.CCR-17-1872

Translational Relevance

Although neuroendocrine prostate cancer (NEPC) is recognized as a lethal disease, the molecular mechanisms underlying its development remain poorly understood. Recently, the concurrent overexpression and gene amplification of MYCN and AURKA have been implicated in the pathogenesis of NEPC. Here, we used a bioinformatics approach to show that a MYCN–PARP–DDR pathway is enriched in CRPC-Neuro, and by mechanism-based experimental approaches, we showed that the MYCN–PARP–DDR pathway is driven by direct MYCN transcriptional regulation of PARP1, PARP2, and DDR genes. Identification of the pathway redefines the molecular phenotype for NEPC and points to a novel set of prognostic and predictive biomarkers. In addition, demonstrating a direct regulatory connection between N-MYC and DDR signaling establishes a mechanistic foundation for novel, actionable therapy targets for NEPC. On the basis of the MYCN–PARP–DDR pathway, we demonstrated the feasibility of using an AURKA and PARP inhibitor combination therapy strategy in preclinical models of NEPC.

is amplified and/or overexpressed in approximately 40% of NEPC, and also in up to 20% of CRPC without NEPC morphology (4, 6), suggesting that some prostate cancers with adenocarcinoma morphology harbor NEPC driver pathways, including AURKA/MYCN aberrations, which promote the transition to NEPC.

A recent study further demonstrated that N-MYC could drive NEPC initiated from prostate epithelial cells in a tissue regeneration model and was essential for maintenance of NEPC (7). In addition, N-MYC has been linked to the expression of multiple DNA damage response (DDR) genes through direct transcriptional regulation or indirect mechanisms (8, 9). Sequencing efforts in mCRPC have shown that approximately 25% harbor genomic alterations in DDR genes (10), and these alterations have been associated with positive responses to the PARP inhibitor olaparib (11). Interestingly, one of the DDR genes modulated by N-MYC is PARP1 (a coactivator of E2F1; ref. 12), which itself regulates multiple target genes involved in DDR (13, 14), and *MYCN* amplification has been associated with increased sensitivity to PARP inhibitors (15).

In the current study, we investigated MYCN-regulated molecular pathways in CRPC classified by morphologic criteria as adenocarcinoma or neuroendocrine. We sought to define therapeutically relevant mechanistic, molecular interactions of the MYCN–PARP–DDR pathway in NEPC development and develop a combination therapy strategy.

Materials and Methods

Cell lines and patient-derived xenografts

C4-2b4 [from Dr. Gary E. Gallick at MD Anderson Cancer Center (MDACC), Houston, TX] was validated by short tandem repeat DNA fingerprint with the AmpFlSTR Identifier PCR Amplification Kit (Applied Biosystems) in MD Anderson's Characterized Cell Line Core Facility. NCI-H660 was newly purchased from ATCC. PDX144-13C is one of the prostate cancer patient-derived xenografts (PDX) developed at MDACC.

PDX transcriptome sequence data processing and gene expression analysis

Poly(A)-selected RNA transcriptome libraries from 28 tissue samples from prostate cancer PDX models generated at MDACC were sequenced with an Illumina HiSeq 2000 system as described previously (16, 17). The read alignment bam files were name sorted with Samtools, and gene level read counts were summarized using htseq-count. The output contains unambiguously mapped read counts, which were then normalized by DESeq2 to adjust for differences in sequencing depth between samples. The reference CRPC-neuroendocrine (CRPC-Neuro) vector of 70 genes was obtained upon request from Beltran and colleagues (18). It is the mean of normalized FPKM across their 13 pathologically defined CRPC-Neuro samples. Using this reference vector, the Pearson correlation coefficients (NE scores) of 28 PDX models were calculated. With 0.35 as a cutoff, the samples were reclassified as CRPC-adenocarcinoma (CRPC-Adeno, <0.35) and CRPC-Neuro (>0.35).

The expression of DDR-M genes of interest was extracted from normalized data matrix. Two-sample *t* test, comparing NE score classified CRPC-Neuro to CRPC-Adeno, was performed and *P* values were adjusted by Benjamini–Hochberg procedure. The expression of Beltran 70 neuroendocrine genes in PDX data set was also unsupervised clustered and displayed in a heatmap (Fig. 1A). The significantly differentially expressed DDR-M genes were unsupervised clustered and displayed in hierarchical clustering heatmap (Fig. 1–D, FDR $\leq$ 0.05; Fig. 1F and G, FDR $\leq$ 0.15).

Beltran transcriptome sequence data processing and analysis

Forty-nine RNA sequencing (RNA-seq) samples' sequence fastq data were downloaded from dbGap phs000909.v.p1. The quality of raw reads was assessed using FastQC followed by read alignment to hg19 reference genome using spliced aligner TopHat2. The rest of data processing steps are the same as section 1.2. Among these 49 RNA-seq samples, two are from their previous publication. Therefore, principal component analysis was performed to determine batch effect. Because no substantial batch effect was detected, the set of all 49 samples was used for downstream analyses. Forty-seven samples (2 from previous publication were excluded) have been classified into 34 CRPC-Adeno and 13 CRPC-Neuro based on NE scores as indicated by Beltran and colleagues (Supplementary Table S15; ref. 18). Because gene expression is quantified differently from the original article and NE scores are missing for the other two samples, the same strategy was used to recalculate NE scores for all 49 samples using normalized read counts. Using 0.4 as a cutoff, this resulted in 35 CRPC-Adeno and 14 CRPC-Neuro. Differential expression of DDR-M genes of interest, between NE score classified CRPC-Neuro and CRPC-Adeno Beltran samples, was performed in the same way as in the PDX data set. The expression of significant genes (FDR $\leq$ 0.05) was unsupervised clustered and displayed in a heatmap (Fig. 1A). The expression profile of AR, MYCN, and common significant DDR-M genes between Beltran and PDX data sets is also unsupervised clustered and displayed (Fig. 1F and G).

Grasso microarray data processing and analysis

Processed Grasso microarray expression data were obtained from GSE35988. Samples were profiled using two different Agilent Whole Genome Microarrays. Therefore, principal component analysis was used to determine batch effect. Because no obvious batch effect was observed, the two expression matrices, GPL6480

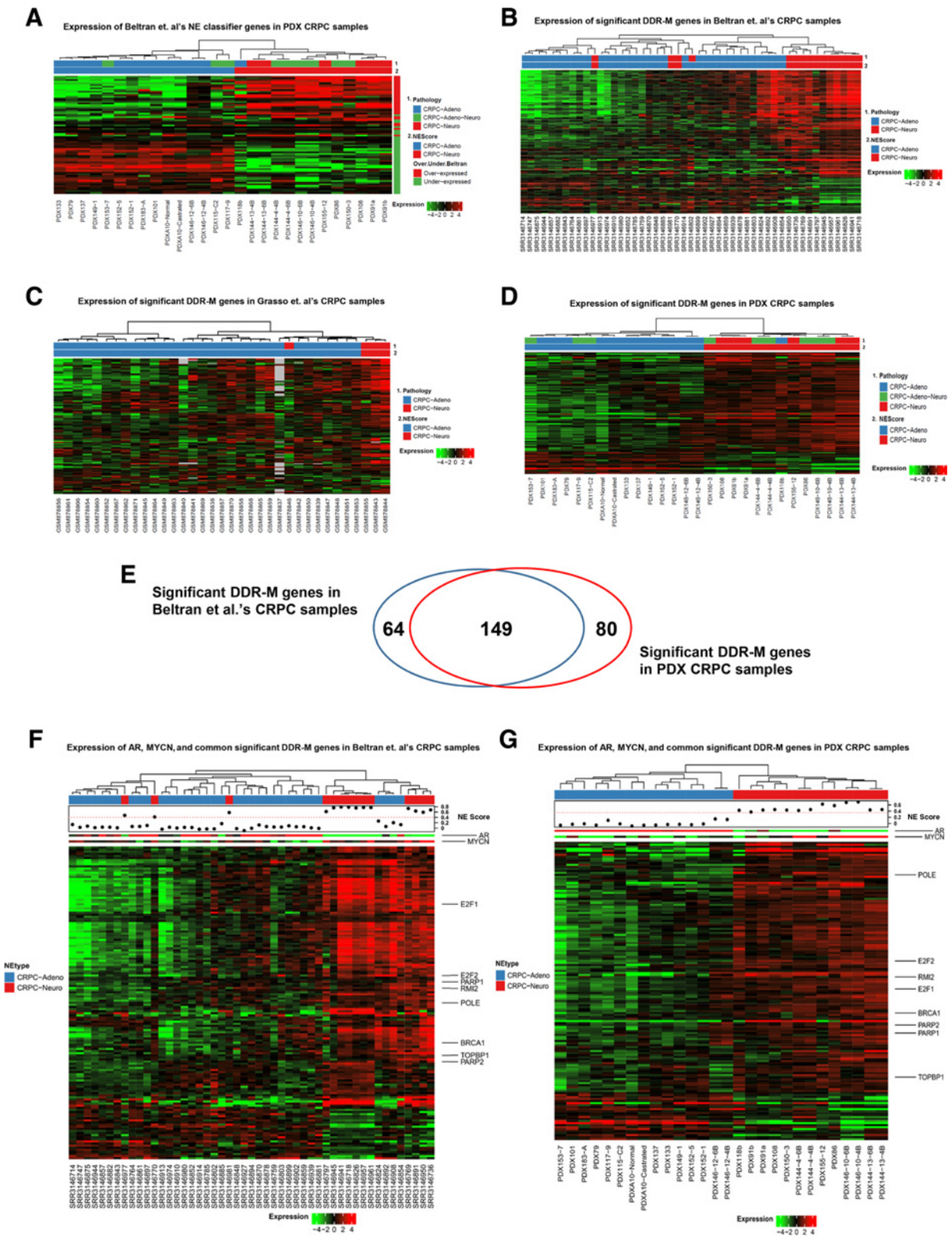

and GPL6848, were combined for downstream analyses. Probes with more than 10 missing values were excluded, and median value was used to quantify gene level expression. As indicated by Beltran and colleagues, to take into account the lower signal-to-noise ratio and also reduced version of NE scores, 0.25 instead of 0.4 was used as a cutoff. This resulted in three CRPC-Neuro samples. The expression of significant genes, derived from differential analysis of PDX data set, was unsupervised clustered and displayed in a heatmap using only CRPC samples (Fig. 1C).

GSE53371 neuroblastoma data processing and unsupervised clustering analysis

The expression matrix and sample information was downloaded from GSE53371. Expression data of AR and MYCN pathway genes are extracted, unsupervised clustered, and displayed in a heatmap (Supplementary Fig. S1).

Quantitative RT-PCR analysis

Total RNA in cells was extracted by TRIzol reagent (Invitrogen) and reverse transcribed into cDNA using High-Capacity cDNA Reverse Transcription Kit (Thermo Fisher Scientific). qRT-PCR was conducted using fast SYBR Green Master Mix (Thermo Fisher Scientific). $2^{-\Delta\Delta C_t}$ method was used to evaluate relative mRNA expressions compared with controls. The primer sequences are listed in Supplementary Table S5.

Western blotting

Total protein in cells was extracted by NP-40 with proteinase inhibitor cocktail. Equal amounts of proteins were loaded and separated by precast gels (Bio-Rad) and transferred to nitrocellulose membranes. After being blocked by nonfat milk, membranes were incubated with primary antibodies against N-MYC (Abcam, ab16898), PARP1 (Santa Cruz Biotechnology, sc-8007), PARP2 (Abcam, ab176330), TOPBP1 (Abcam, ab2402), BRCA1 (Cell Signaling Technology, 9025S), POLE (Santa Cruz Biotechnology, sc-135885), and RMI2 (Abcam, ab122685). Washed membranes were incubated with HRP-conjugated secondary antibodies (1:10,000, Cell Signaling Technology). ECL (Thermo Fisher Scientific) was used to detect immune complexes.

siRNA and plasmid transfection

C4-2b4 and NCI-H660 cells were seeded one day before siRNA transfection. RNA and protein extracts were prepared, and biological assays were performed 48 hours after siRNA transfection. siRNA sequences are listed in Supplementary Table S6. The *MYCN* (clone ID: OHu27902, Genscript), *PARP1* (clone ID: OHu25551, Genscript) plasmid, and the control vector were transfected into C4-2b4 and NCI-H660 cells by X-tremeGENE HP DNA transfection reagent (Roche). Protein extracts were prepared 72 hours after plasmid transfection.

ChIP assay

Chromatin immunoprecipitation (ChIP) assays were performed using the SimpleChIP Plus Enzymatic Chromatin IP Kit (Cell Signaling Technology). Chromatin was immunoprecipitated using anti-N-MYC (Abcam, ab16898) antibody. Anti-histone H3 antibody (Cell Signaling Technology) and normal rabbit IgG (Cell Signaling Technology) were used as positive control and negative control, respectively. ChIP-derived DNA was quantified using qRT-PCR and also electrophoresed on 2% agarose gels. The primer sequences are provided in Supplementary Table S7.

MTS assay

MTS assay was performed using MTS CellTiter 96 AQueous One Solution Cell Proliferation Assay (Promega) and a microplate reader (BioTek). Relative absorbance at 490 nm was used as function of cell viability/proliferation.

Colony assay

For siRNA assay, cells were trypsinized 24 hours after siRNA transfection and seeded into 6-well plates at low density (2×10^4/well) and grown for up to 2 weeks for colony formation. For drug assay, cells were seeded into 6-well plates at a low density as described above and then treated with drug for up to 2 weeks for colony formation. Cell culture medium containing drug or DMSO was renewed every 3 days. Colonies were fixed with cold methanol and then stained with 0.5% crystal violet. The number of colonies was counted and imaged with a microscope using NIS-Elements AR2.30 software (Nikon).

Flow cytometry assay

Cells were harvested 48 hours after siRNA transfection or drug treatment, stained with propidium iodide, and analyzed using the FACSCanto II flow cytometer (BD Biosciences). Quantitative data were obtained using FlowJo software (TreeStar Inc.).

Scratch assay

For siRNA assay, a straight longitudinal incision was made on the monolayer of cells using a pipette tip 24 hours after siRNA transfection. After change of culture medium, cells were incubated for an additional 48 hours. For drug assay, drug treatment was applied

Figure 1.

Increased DNA damage response and mitotic gene expression in CRPC-Neuro samples. **A,** Unsupervised clustering of Beltran 70 classifier genes in PDX RNA-seq data set. Samples were classified into CRPC-Neuro and CRPC-Adeno using NE scores. The pathology and NE score classifications are shown in top covariate bars. The over (in red) and under (in green) expression status of these genes in CRPC-Neuro samples (also see Supplementary Table S2) is shown on the right covariate bar. **B,** Unsupervised clustering of significant DDR-M genes in Beltran et al. RNA-seq data set. The DDR-M significant genes (FDR $\leq$ 0.05) are derived from differential analysis comparing NE score classified CRPC-Neuro to CRPC-Adeno Beltran et al. samples. The pathology and NE score classifications are shown in top covariate bars. **C,** Unsupervised clustering of significant DDR-M genes in Grasso et al. microarray data set. The DDR-M significant genes (FDR $\leq$ 0.05) are derived from differential analysis comparing NE score classified CRPC-Neuro with CRPC-Adeno samples. The pathology and NE score classifications are shown in top covariate bars. **D,** Unsupervised clustering of significant DDR-M genes in PDX RNA-seq data set. The DDR-M significant genes (FDR $\leq$ 0.05) are derived from differential analysis comparing NE score classified CRPC-Neuro with CRPC-Adeno PDX samples. The pathology and NE score classifications are shown in top covariate bars. **E,** Significant DDR-M genes in Beltran and PDX data sets at FDR 0.15 were compared, and 149 common genes were identified. **F,** Unsupervised clustering of AR, MYCN, and common significant DDR-M genes (FDR $\leq$ 0.15) in Beltran et al. RNA-seq data set. The NE score classifications (CRPC-Neuro and CRPC-Adeno) are shown in top covariate bar. The NE score for each sample is shown in covariate scatter plot with 0.4 as the cutoff. **G,** Unsupervised clustering of AR, MYCN, and common genes (FDR $\leq$ 0.15) in PDX data set. The NE score classifications (CRPC-Neuro and CRPC-Adeno) are shown in top covariate bar. The NE score for each sample is shown in covariate scatter plot with 0.35 as the cutoff.

immediately after the incision and maintained for 48 hours. Cells were fixed, counted, and imaged as described in colony assay.

Xenograft model

A total of 5×10^6 C4-2b4 cells mixed with high protein Matrigel were injected subcutaneously to nude mice. For MDACC PDX 144-13C cells, equal sized tumors were implanted subcutaneously to previously castrated SCID male mice. The mice were randomly divided to receive vehicle control, PHA-739358 (15 mg/kg/d every day i.p.), olaparib (40 mg/kg/day, 5 days each week, i.p.), or concomitant olaparib and PHA-739358 when the tumor volume reached 30 to 50 mm^3. Tumors were measured twice a week after the initiation of the treatment. C4-2b4 tumors were harvested on day 18, and MDACC PDX 144-13C tumors were harvested on day 21.

Human prostate cancer tissues and histochemical analysis

Twenty-four human prostate cancer specimens were obtained from the MD Anderson Prostate Tissue Bank. The specimens consisted of primary tumors including 18 adenocarcinomas (Adeno), five small-cell carcinomas [small cell prostate cancer (SCPC)], and one mixed Adeno/NEPC. The specimens were derived from radical prostatectomy ($n = 14$), cystoprostatectomy ($n = 8$), pelvic exenteration ($n = 1$), and transurethral resection specimens ($n = 1$). Specimens are from untreated patients (6 Adeno) and patients previously treated with hormonal ablation alone (6 Adeno) or hormonal ablation in combination with other therapies (6 Adeno, 5 SCPC, 1 mixed Adeno/NEPC), and were referred to as ADT. Formalin-fixed paraffin-embedded tissue slides were prepared, and MYCN mRNA expression was analyzed by ISH using the viewRNA-ISH system (Affymetrix). Expression of PARP1, PARP2, TopBP1, and BRCA1 was analyzed using IHC.

Statistical analysis

Data were presented as the mean ± SD. The Wilcoxon rank-sum test was used for data with nonnormal distributions or data with small sample sizes, such as qRT-PCR analyses, ChIP assay, MTS assay, colony assay, flow cytometry assay, and scratch assay. ANOVA *t* test was used for analysis of tumor growth and tumor wet weights. $P < 0.05$ was considered statistically significant.

Results

DDR-mitotic genes are enriched in CRPC-Neuro

Previous studies demonstrated that DDR and mitotic/cell-cycle genes are enriched in mCRPC (10, 19). We developed a gene set comprised of 195 DDR genes (http://gather.genome.duke.edu, GO:0006974),180 mitotic cell-cycle genes (http://gather.genome.duke.edu, GO:0000278), and 31 additional DDR- or mitosis-related genes (http://www.informatics.jax.org), that is, DDR-M genes (Supplementary Table S1) to analyze the molecular phenotype in mCRPC. There were 79 genes that overlapped between the DDR gene set and mitotic cell-cycle gene set. To determine the role of DDR-M genes in divergent evolution process of CRPC-Neuro from CRPC-Adeno, we performed bioinformatics analysis using two public human prostate cancer data sets (10, 18), and RNA-seq data generated from MDACC PDX prostate cancer models, which were derived from CRPC-Adeno and CRPC-Neuro prostate cancer (20, 21). The tissue samples from 28 MDACC PDX prostate cancer models were assigned to CRPC-Adeno and CRPC-Neuro phenotypes on the basis of the 70-gene expression molecular classifier generated by Beltran and colleagues (Fig. 1A; Supplementary Table S2; ref. 18). The significantly differentially expressed DDR-M genes in the three data sets ($P_{adj} < 0.05$) were analyzed by unsupervised clustering and shown in hierarchical clustering heatmap (Fig. 1B–D; Supplementary Table S3). Similar DDR-M gene expression patterns are seen in these three data sets, which show upregulation of a majority (~75%) of DDR-M genes and downregulation of a smaller portion (~25%) of DDR-M genes. The data suggested a correlation between upregulation of DDR-M gene expression and CRPC-Neuro development.

To gain insight into the role of DDR-M genes in CRPC-Neuro development, we compared 213 significantly differentially expressed DDR-M genes in Beltran and colleagues' CRPC data set (18) with 229 significantly differentially expressed DDR-M genes in PDX CRPC data set and identified 149 significantly differentially expressed DDR-M genes common in Beltran and colleagues' CRPC and PDX CRPC (Fig. 1E; Supplementary Table S4). In the unsupervised clustering analysis of AR, MYCN, and these common significant DDR-M genes, we found that the upregulation of the majority of DDR-M genes in CRPC-Neuro is positively correlated with loss of/reduced AR expression and increased MYCN expression (Fig. 1F and G). On the basis of the results of previous studies (8, 9, 12–15, 22, 23), and our N-MYC–binding site analysis (data not shown), a small group of DDR-M genes was selected (genes indicated in Fig. 1F and G and shown in Fig. 2A), that is, MYCN-PARP1/2-DDR signaling pathway genes, for further analysis.

N-Myc transcriptionally activates PARP1/2 and drives DDR signaling

Gene expression analysis showed that N-MYC levels were increased in CRPC-Neuro compared with CRPC-Adeno and that associations between N-MYC and PARP1/2-DDR signaling pathway genes were uniformly higher in CRPC-Neuro compared with CRPC-Adeno (Fig. 2A). These data together with our analysis of predicted N-MYC–binding sites (data not shown) suggested a possible role for the MYCN–PARP1/2-DDR signaling pathway in the phenotypic transition from CRPC-Adeno to CRPC-Neuro (Fig. 2A).

To assess a possible role for the MYCN–PARP1/2-DDR signaling pathway in an independent, MYCN-driven malignancy, we analyzed a public data set from neuroblastoma tissue samples that included *MYCN*-amplified and *MYCN* normal copy number tumors (24). The results showed that MYCN–PARP1/2-DDR pathway genes were significantly upregulated in *MYCN*-amplified neuroblastoma compared with *MYCN* normal copy number neuroblastoma tumors (Supplementary Fig. S1). To determine expression of MYCN–PARP1/2-DDR pathway genes in human prostate adenocarcinoma (untreated and androgen deprivation therapy treated), and NE/SCPC tissues, we performed MYCN *in situ* hybridization (ISH) or PARP1/2, BRCA1, and TOPBP1 immunostaining. The results demonstrated negative N-MYC mRNA expression in untreated adenocarcinoma (0/6; Fig. 2B). In ADT-treated adenocarcinoma, 2 of 12 samples showed detectable N-MYC mRNA (Fig. 2C). In contrast, N-MYC mRNA was expressed in 2 of 5 ADT-treated SCPC samples (Fig. 2D and E), and one mixed Adeno/NE sample (not shown). Although statistically significant comparisons between ADT-Adeno and ADT-SCPC were not achievable due to the small sample size, higher levels of PARP1/2-DDR pathway proteins tended to be found in

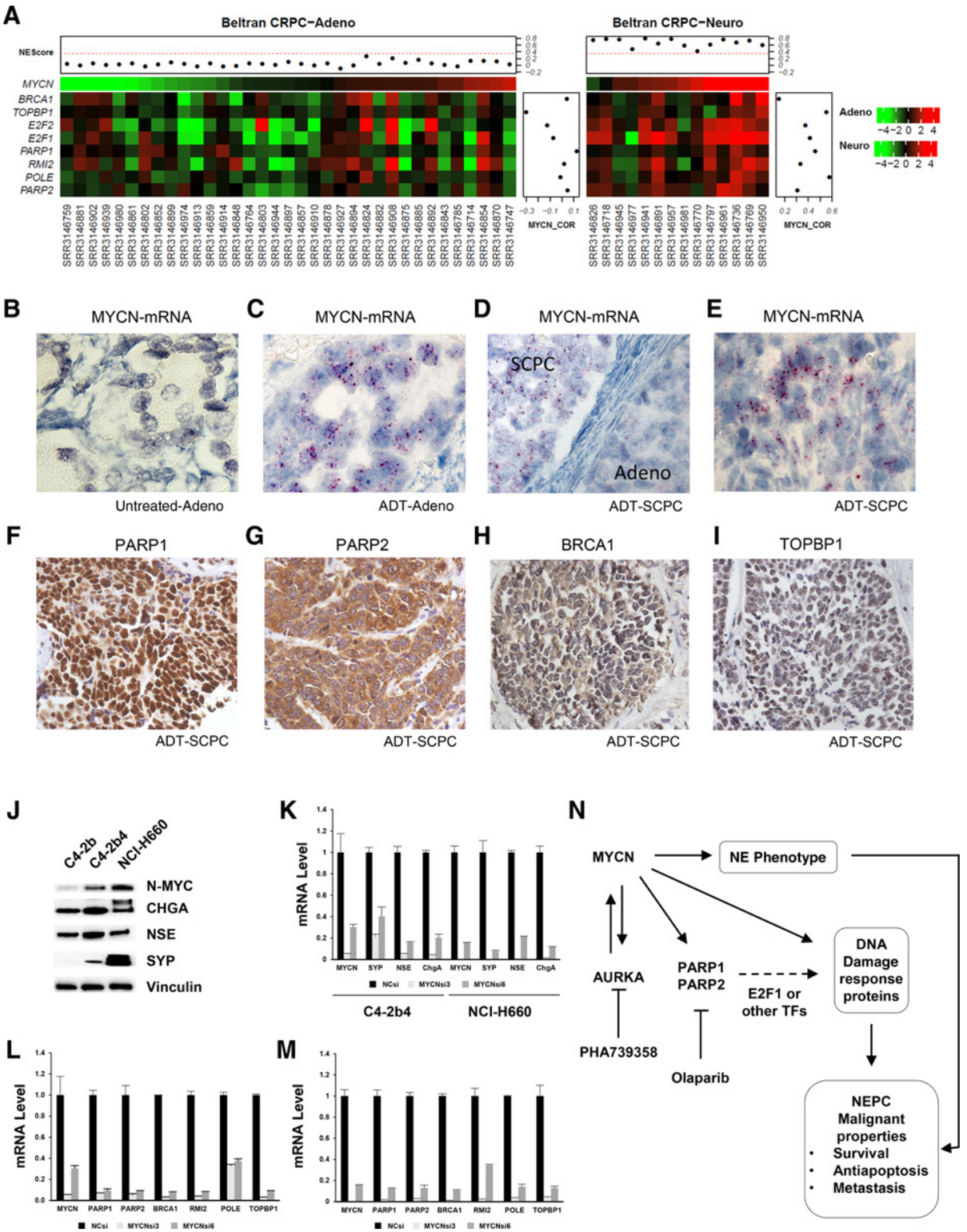

Figure 2.

Analysis of proposed MYCN–PARP–DDR signaling pathway. **A,** The expression pattern of MYCN pathway genes in Beltran CRPC-Adeno (left, heatmap) and CRPC-Neuro (right, heatmap) are shown. The samples are ordered on the basis of MYCN expression level. The top covariate bars indicate neuroendocrine scores. The Pearson correlation coefficients of pathway genes with MYCN expression are shown in the box plot next to heatmap. **B,** MYCN ISH in untreated adenocarcinoma. **C,** MYCN ISH in ADT-treated adenocarcinoma or in SCPC (**D** and **E**). In one SCPC sample, MYCN expression in some cancer cells with adenocarcinoma morphology was lower than that in adjacent SCPC cells (right in **D**). **F–I,** Positive PARP1, PARP2, BRCA1, and TOPBP1, respectively, in SCPC. **J,** Western blot analysis of N-MYC and NE markers in C4-2b, C4-2b4, and NCI-H660. **K–M,** Effect of MYCNsi on mRNA expression of MYCN–PARP–DDR pathway genes in C4-2b4 and NCI-H660. **N,** Proposed MYCN–PARP–DDR signaling pathway.

ADT-SCPC tissues with MYCN positivity (Fig. 2F–I). To test the molecular connections within the MYCN–PARP1/2-DDR signaling pathway genes, we selected C4-2b4, an AR-positive, androgen-independent, and N-MYC–positive CRPC subline derived from C4-2b, and NCI-H660, an NEPC cell line, for mechanistic analysis. Western blotting analysis showed that C4-2b4 expresses markedly higher N-MYC and neuroendocrine markers chromogranin A (CHGA), neuron-specific enolase (NSE), and synaptophysin (SYP) than parental C4-2b (Fig. 2J), suggesting that it may potentially be a CRPC-Adeno precursor to NEPC. qRT-PCR analysis demonstrated that knockdown of *MYCN* with siRNA suppressed the expression of neuroendocrine markers SYP, NSE, CHGA, and MYCN–PARP–DDR pathway genes, including PARP1/2, BRCA1, RMI2, POLE, and TOPBP1 in C4-2b4 and NCI-H660 (Fig. 2K–M). Our results led us to consider that MYCN drives the phenotypic transition from CRPC-Adeno to CRPC-Neuro through a MYCN–PARP1/2-DDR pathway, in which MYCN transcriptionally regulates PARP1/2 and specific DDR genes directly or through regulation of E2F1 (Fig. 2N).

To provide mechanistic support for potential N-Myc transcriptional regulation of MYCN–PARP1/2-DDR pathway, we performed ChIP assays to determine whether N-MYC can directly bind putative N-MYC target genes in the MYCN–PARP1/2-DDR pathway, including PARP1, PARP2, BRCA1, RMI2, and TOPBP1. Multiple putative N-MYC–binding sites for each gene promoter were analyzed, including four N-MYC–binding sites, within 1,600 bp upstream of the PARP1 transcriptional start site, two binding sites within 1,000 bp upstream of the PARP2 transcriptional start site, two binding sites within 900 bp of the BRCA1 transcriptional start site, three binding sites within 1,300 bp of the RMI2 transcriptional start site, and one binding site within 1,900 bp of the TOPBP1 transcriptional start site (Fig. 3A and B). We designed primers to amplify 82bp-225bp segments spanning each predicted binding site. In C4-2b4, the results of qRT-PCR (Fig. 3C–G) and RT-PCR (Fig. 3H) analyses confirmed that N-MYC directly binds the promoter regions of PARP1, PARP2, BRCA1, RMI2, and TOPBP1. Specifically, we experimentally validated P1BS2, P1BS4, and P2BS1 N-MYC–binding sites for PARP1 and PARP2, respectively (Fig. 3C, D, and H), B1BS1 for BRCA1 (Fig. 3E and H), R2BS2 for RMI2 (Fig. 3F and H), and T1BS1 for TOPBP1 (Fig. 3G and H). In H660, the results of qRT-PCR (Fig. 3I–M) and RT-PCR (Fig. 3N) were similar to those in C4-2B4, except that all the four predicted binding sites on PARP1 promoter (P1BS1, P1BS2, P1BS3, and P1BS4) were bound by N-Myc (Fig. 3I and N).

The cooperative oncogenic effects of N-MYC and PARP are inhibited by gene knockdown *in vitro*

We used *MYCN* and/or *PARP1/2* knockdown to determine the effects of MYCN and PARP1/2 on MYCN–PARP–DDR signaling and cancer cell activities in C4-2b4 and NCI-H660. Western blotting analysis showed that key pathway components (PARP1/2, BRCA1, RMI2, POLE, and TOPBP1) were downregulated by MYCNsi in C4-2b4 (Fig. 4A, left) and NCI-H660 (Fig. 4B, left), consistent with qRT-PCR results (Fig. 2E and F). Moreover, knockdown of *PARP1/2* also led to reduction of BRCA1, RMI2, POLE, and TOPBP1 protein expression (Fig. 4A and B, right). Specifically, BRCA1, RMI2, and TOPBP1 were substantially suppressed by PARP1si and PARP2si in C4-2b4 (Fig. 4A) and were also suppressed by PARP1si and PARP2si in various magnitudes in NCI-H660 (Fig. 4B). To support these results, we overexpressed MYCN and PARP1 in C4-2b4 and H660 cells and analyzed BRCA1, RMI2, POLE1, and TOPBP1 expression. The results showed increased expression of all selected DDR genes in response to enforced MYCN or PARP1 expression (Fig. 4C). Analysis of the downstream biological effects of MYCNsi, PARP1si, and PARP2si treatment in C4-2b4 cells showed reduced colony formation (Fig. 4D) and cell migration in scratch assays (Fig. 4E), indicating extensive downstream activities of the MYCN–PARP1/2-DDR pathway. It is notable that the combination of MYCN and PARP1/2 knockdown achieved significantly greater effects in these biological assays compared with any single siRNA transfection (Fig. 4D and E). To determine whether DNA damage regulation may play a role in MYCN–PARP1/2-DDR pathway activities, we analyzed γ-H2AX levels following MYCNsi treatment and demonstrated that suppression of N-MYC levels led to increased DNA damage in C4-2b4 and H660 cells (Fig. 4F). Analysis of the downstream biological effects induced by MYCNsi, PARP1si, and PARP2si showed reduced cell viability/proliferation in the C4-2b4 (Fig. 4G) and H660 (Fig. 4I) models, and increased percentage of sub-G_1 cells in the C4-2b4 (Fig. 4K) and H660 (Fig. 4M) models. Importantly, BRCA1si and RMIsi also reduced cell viability/proliferation and increased percentage of sub-G_1 cells in the C4-2b4 (Fig. 4H and L), and H660 (Fig. 4J and N) models.

Combined AURKA and PARP inhibition significantly suppresses cancer cell activities *in vitro* and xenograft tumor growth *in vivo*

Previous studies demonstrated that stabilization of N-MYC was a critical function of AURKA (25). Therefore, we sought to test whether combined AURKA and PARP inhibition would maximally suppress the MYCN–PARP–DDR pathway. Inhibition of AURKA with PHA739358 (PHA) or inhibition of PARP with olaparib suppressed PARP1/2, BRCA1, RMI2, POLE, and TOPBP1 at different magnitudes, while inhibition of AURKA with PHA together with inhibition of PARP with olaparib resulted in greater downregulation of these DDR proteins (Fig. 5A and B).

We performed various biological assays to assess whether the combination of PHA and olaparib can generate cooperative effects on prostate cancer cells. In the two prostate cancer cell lines used, monotherapy with PHA or olaparib increased the proportion of sub-G_1 cells (Fig. 5C and G) and reduced viability/proliferation (Fig. 5D and H), colony formation (Fig. 5E), and cell migration in scratch assays (Fig. 5F). PHA achieved better treatment effects than olaparib as a monotherapy agent. Importantly, PHA together with olaparib generated significantly better therapeutic effect (Fig. 5C–H).

To test the therapeutic effect of PHA and olaparib combination treatment strategy *in vivo*, we analyzed PHA or olaparib alone and PHA + olaparib combination treatment using a subcutaneous cell line model (C4-2b4, an N-MYC–positive CRPC-Adeno to CRPC-Neuro transition model) and a subcutaneous CRPC-Neuro PDX tumor model (MDACC PDX144-13C, in precastrate SCID mice). In both models, treatment with PHA or olaparib alone was sufficient to suppress tumor growth, indicated by reduced tumor volumes (Fig. 5I and K) and tumor weights (Fig. 5J and L), with comparable efficacy. The combination of PHA and olaparib achieved significantly greater tumor suppression than treatment with olaparib or PHA alone (Fig. 5I–L).

A

Predicted N-MYC–binding sites

Promoter	Site ID	Start	End	Predicted site sequence
PARP1	P1BS1	−1533	−1526	GGCACCTG
	P1BS2	−1078	−1071	GCCAGGTG
	P1BS3	−986	−979	GCAACATG
	P1BS4	−59	−52	GCCCCGTG
PARP2	P2BS1	−922	−915	GCCCCATG
	P2BS2	−208	−201	AGCTCGTG
BRCA1	B1BS1	−899	−892	ACCACTTG
	B1BS2	−269	−262	GCCACCTG
RMI2	R2BS1	−1258	−1251	ACCAGGTG
	R2BS2	−187	−180	ACCACGTG
	R2BS3	−7	0	ACCACGCG
TOPBP1	T1BS1	−1844	−1837	AGCACGTG

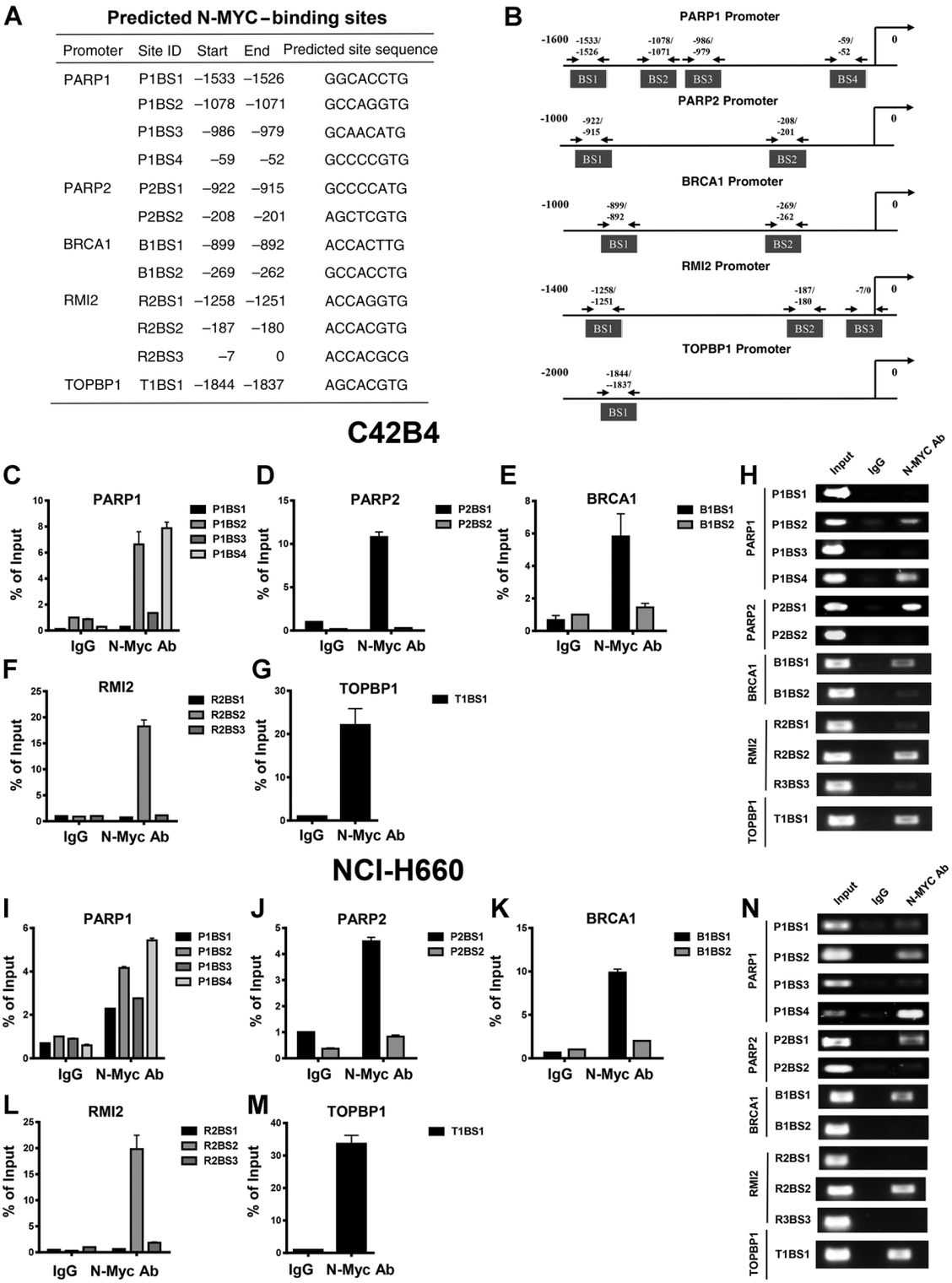

Figure 3.

ChIP-PCR analysis of N-MYC binding to PARP1/2 and selected DDR-M genes. **A** and **B,** Predicted N-MYC–binding sites on PARP1, PARP2, BRCA1, RMI2, and TOPBP1 promoters according to JASPAR database. **C–G,** ChIP-PCR assay testing the direct binding of N-MYC to PARP1, PARP2, BRCA1, RMI2, and TOPBP1 promoter in C4-2b4. **I–M,** ChIP-PCR assay testing the direct binding of N-MYC to PARP1, PARP2, BRCA1, RMI2, and TOPBP1 promoter in H660. **H** and **N,** DNA gel electrophoresis were conducted to confirm N-MYC occupancy on PARP1, PARP2, BRCA1, RMI2, and TOPBP1 promoter C4-2b4 and NCI-H660. P1, PARP1; P2, PARP2; B1, BRCA1; R2, RMI2; T1, TOPBP1; BS, binding site.

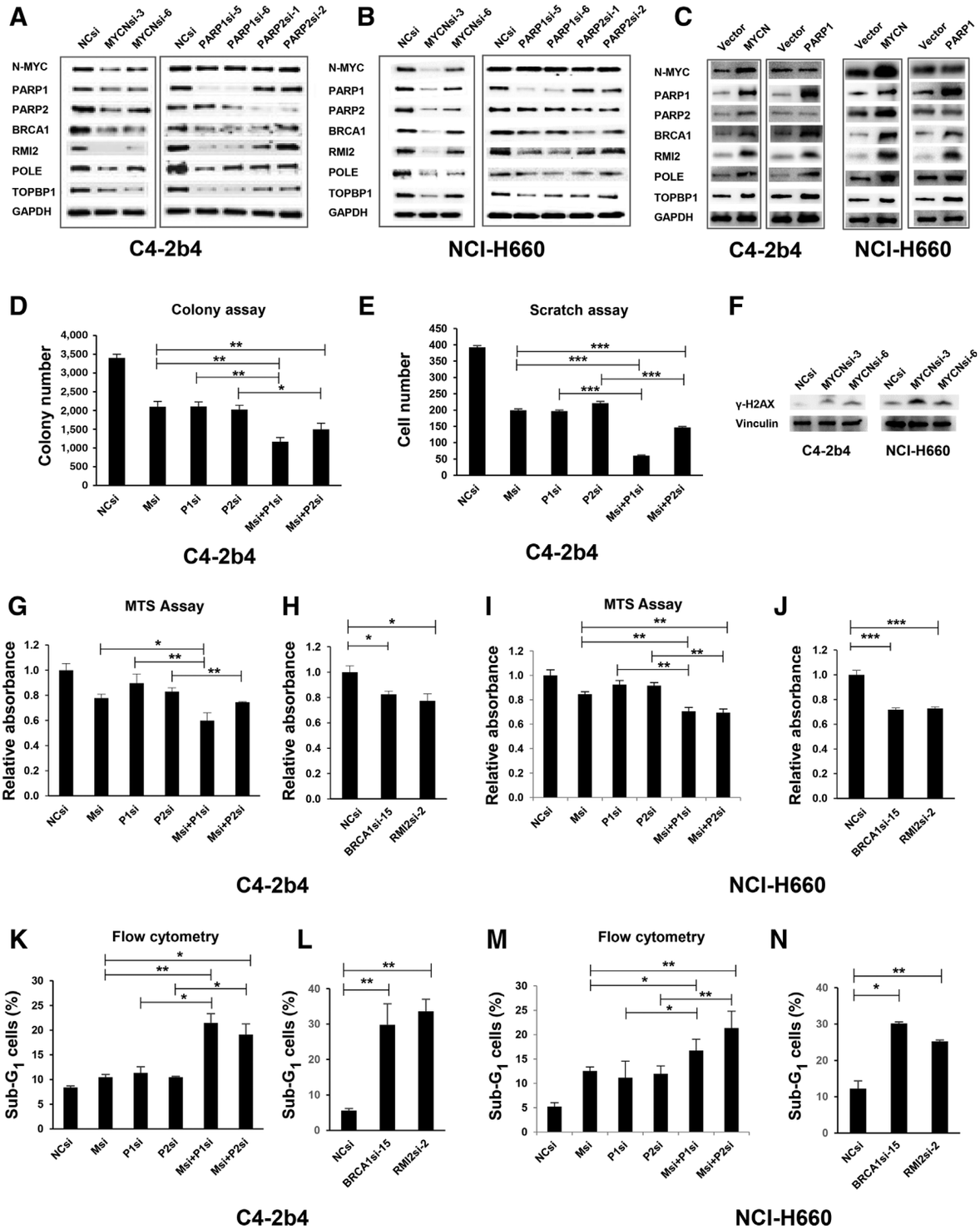

Figure 4.

Effect of *MYCN* and/or *PARP* knockdown on MYCN–PARP–DDR pathway and CRPC oncogenic activities. **A** and **B,** Effect of MYCNsi, or PARP1/2si on protein expression of MYCN–PARP–DDR pathway genes in C4-2b4 and NCI-H660. **C,** Effect of MYCN or PARP1 overexpression on protein levels of MYCN–PARP–DDR pathway genes in C4-2b4 and NCI-H660. **D** and **E,** Colony growth and cell migration after cooperative oncogenic effects of N-MYC and PARP by genetic knockdown in C4-2b4 cells. **F,** Effect of MYCNsi on protein expression of γ-H2AX. **G** and **I,** Cell proliferation/viability (**K** and **M**) sub-G_1 cell distribution in C4-2b4 and H660 cells transfected with MYCNsi, PARP1/2si, or MYCNsi + PARP1/2si. **H** and **J,** Cell proliferation/viability (**L** and **N**) sub-G_1 cell distribution in C4-2b4 and H660 cells transfected with BRCA1si and RMI2si. In **D–M**, Msi, MYCNsi; P1si, PARP1si; P2si, PARP2si. *, $P < 0.05$; **, $P < 0.01$; ***, $P < 0.001$ (*t* test).

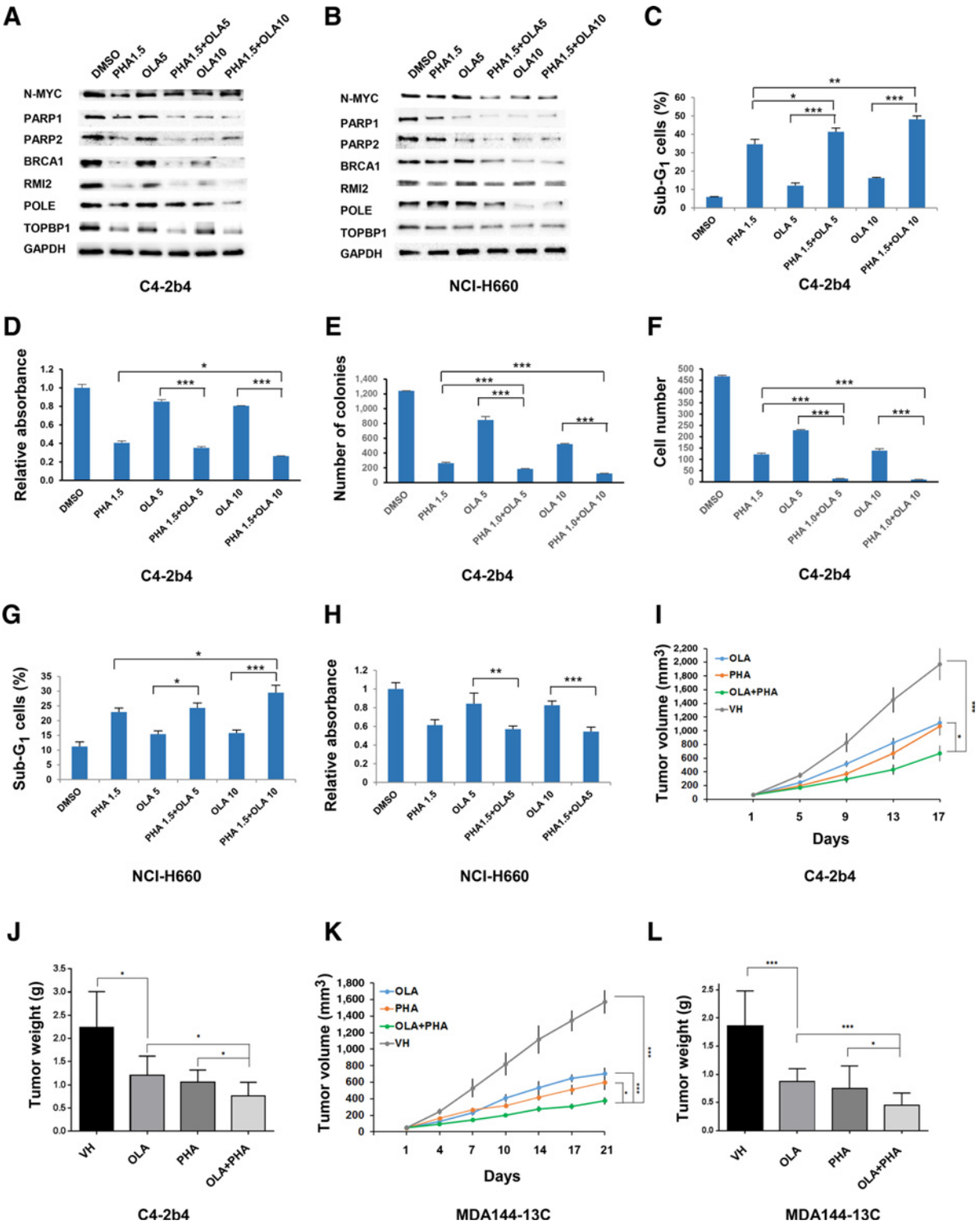

Figure 5.

AURKA and PARP inhibitors cooperatively suppress prostate cancer oncogenic activities *in vitro* and xenograft tumor growth *in vivo*. **A** and **B,** Effect of PHA, OLA, and combination of PHA and OLA on protein expression of MYCN–PARP–DDR pathway genes in C4-2b4 and NCI-H660 cells. PHA1.5, PHA 1.5 μmol/L; OLA5, OLA 5 μmol/L; OLA10, OLA 10 μmol/L. **C–H,** Demonstration of the cooperative oncogenic effects of N-MYC and PARP by pharmacologic inhibition of AURKA and PARP in C4-2b4 and NCI-H660 cells. PHA1.5, PHA 1.5 μmol/L; OLA5, OLA 5 μmol/L; OLA10, OLA 10 μmol/L. Sub-G_1 cell distribution (**C** and **G**), cell proliferation/viability (**D** and **H**), colony growth (**E**), and cell migration (**F**) in C4-2b4 and/or H660 cells treated with AURKA inhibitor PHA, PARP inhibitor OLA, or PHA + OLA. **I–L,** Results from C4-2b4 and MDACC 144-13C subcutaneous model. **I,** Tumor growth curve for C4-2b4. **J,** Tumor wet weight for C4-2b4. **K,** Tumor wet weight for MDACC prostate cancer 144-13C. **L,** Tumor growth curve for MDACC prostate cancer 144-13C. *, $P < 0.05$; **, $P < 0.01$; ***, $P < 0.001$ (*t* test).

Discussion

Previous studies have demonstrated a critical role for N-MYC in the development of NEPC (4, 6–9). It is noteworthy that MYCN is overexpressed in approximately 5% to 20% of prostatic adenocarcinomas in clinical samples (4, 6). In our analyses, N-MYC mRNA was identified as being increased relative to mean of all samples in 13% (2/15) of CRPC-Adeno PDXs (Fig. 1G) and 17% (2/12) ADT-treated adenocarcinomas (Fig. 2C). Together, these data suggest that there is a subset of CRPC-Adeno that may gain certain molecular characteristics of NEPC before their transition to CRPC-Neuro. Our study reveals a MYCN–PARP–DDR signaling pathway in CRPC-Neuro, and a subset of CRPC-Adeno that likely represents a precursor to CRPC-Neuro. We identified PARP1, PARP2, BRCA1, RMI2, and TOPBP1 as direct N-MYC targets and linked N-MYC and PARP with the expression of multiple important DDR-M genes, such as BRCA1, RMI2, POLE, and TOPBP1. We further showed that suppression of MYCN–PARP–DDR pathway genes, including BRCA1 and RMI2, led to reduced cell survival and increased percentage of sub-G_1 cells. To our knowledge, elucidation of such an extensive and direct mechanistic link of N-MYC to PARP and DDR functions is novel and establishes mechanism-based therapy targets that are currently actionable. Although AURKA inhibitors have shown limited clinical efficacy as single agents in solid tumors, including CRPC, selecting patients with specific DDR gene alterations or *MYCN* amplification may increase their response rate, as single agents and in combination with PARP inhibition (26). Our mechanistic studies also provide a strong rationale to target N-MYC with AURKA inhibitor (destabilizing N-MYC) and downstream DDR-M signaling with PARP inhibitor in a combination treatment approach for NEPC. In addition, our strategy would be relevant to the treatment of "aggressive-variant prostate cancer," an AR inhibitor–refractory, identifiable phenotype that is clinically more prevalent than NEPC (20).

PARP1 is well known as a chromatin-associated enzyme, which modifies various nuclear proteins by poly(ADP-ribosyl)ation. In addition to its enzymatic activity, PARP1 also functions as a coactivator for many important transcription factors, including E2F1 (12) and NF-κB (27). The results of our studies reveal the following novel findings with regard to the functions of PARP1/2 within the context of the MYCN–PARP–DDR pathway. First, N-MYC directly targets PARP1/2, which, in turn, may mediate N-MYC signaling in NEPC development. Second, as knockdown of *PARP1/2* led to downregulation of BRCA1, RMI2, POLE, and TOPBP1, it should be considered that PARP1/2 may regulate transcription coactivator functions for these specific genes.

Kumar and colleagues reported that CRPC patients with high cell-cycle progression scores demonstrated increased expression of Fanconi anemia complex components and that suppression of these genes led to reduced proliferation and increased DNA damage in prostate cancer cell lines. In this report, the authors also showed that patients with a deleterious event in any Fanconi anemia pathway component or ATM gene demonstrated responses to PARP inhibition (28). Our recent publication showed increased HR gene expression in CRPC and that suppression of a subset of these HR genes led to potentiation of PARP inhibitor-mediated cytotoxicity (23). In this current study, we show that two of these HR genes, that is, BRCA1 and RMI2, are transcriptionally activated by N-MYC, and that BRCA1 and RMI2 knockdown led to significant reductions in cell survival/proliferation and increased percentages of sub-G_1 cells in our CRPC-Adeno and CRPC-Neuro cell line models. In addition, combination AURKA and PARP inhibition suppressed growth in the C4-2b4 xenograft model and the Neuro PDX144-13C model. Taken together, the results of these recent publications suggest that DDR gene upregulation contributes to the CRPC and/or NEPC phenotypes and that MYCN–PARP–DDR signaling can drive these activities under experimental conditions.

On the basis of our results, we suggest that the combination of AURKA inhibition and PARP inhibition is a viable strategy for clinical testing. In addition, the clinical efficacy of this combination approach may be enhanced by patient selection based on specific DDR gene alterations or increased MYCN–PARP–DDR signaling activities. Further investigation of N-MYC DDR gene targets will more fully elucidate the importance of the MYCN–PARP–DDR signaling pathway in the development and maintenance of NEPC.

Disclosure of Potential Conflicts of Interest

No potential conflicts of interest were disclosed.

Authors' Contributions

Conception and design: W. Zhang, B. Liu, L. Li, A.K. Azad, A.M. Aparicio, A.M. Chinnaiyan, T.C. Thompson

Development of methodology: W. Zhang, B. Liu, W. Wu, L. Li, S.P. Basourakos, G. Yang, A.K. Azad, X. Cao

Acquisition of data (provided animals, acquired and managed patients, provided facilities, etc.): W. Zhang, B. Liu, W. Wu, L. Li, S.P. Basourakos, D. Korentzelos, Y. Luan, G. Yang, S. Park, A.K. Azad, X. Cao, C.J. Logothetis, N. Navone, P. Troncoso

Analysis and interpretation of data (e.g., statistical analysis, biostatistics, computational analysis): W. Zhang, B. Liu, W. Wu, L. Li, B.M. Broom, S.P. Basourakos, D. Korentzelos, Y. Luan, G. Yang, A.K. Azad, J. Kim, C.J. Logothetis, P. Troncoso, T.C. Thompson

Writing, review, and/or revision of the manuscript: W. Zhang, B. Liu, W. Wu, L. Li, B.M. Broom, G. Yang, A.K. Azad, J. Kim, P.G. Corn, A.M. Aparicio, A.M. Chinnaiyan, T.C. Thompson

Administrative, technical, or material support (i.e., reporting or organizing data, constructing databases): J. Wang, G. Yang, S. Park, C.J. Logothetis, N. Navone, T.C. Thompson

Study supervision: T.C. Thompson

Acknowledgments

This research was supported by MD Anderson NCI Prostate Cancer SPORE Grant P50 CA140388 and the NCI Cancer Center Support Grant P30 CA16672.

The costs of publication of this article were defrayed in part by the payment of page charges. This article must therefore be hereby marked *advertisement* in accordance with 18 U.S.C. Section 1734 solely to indicate this fact.

Received June 30, 2017; revised October 20, 2017; accepted November 8, 2017; published OnlineFirst November 14, 2017.

References

1. Wang HT, Yao YH, Li BG, Tang Y, Chang JW, Zhang J. Neuroendocrine prostate cancer (NEPC) progressing from conventional prostatic adenocarcinoma: factors associated with time to development of NEPC and survival from NEPC diagnosis-a systematic review and pooled analysis. J Clin Oncol 2014;32:3383–90.
2. Helpap B, Kollermann J, Oehler U. Neuroendocrine differentiation in prostatic carcinomas: histogenesis, biology, clinical relevance, and future therapeutical perspectives. Urol Int 1999;62:133–8.
3. Palmgren JS, Karavadia SS, Wakefield MR. Unusual and underappreciated: small cell carcinoma of the prostate. Semin Oncol 2007;34:22–9.

4. Beltran H, Rickman DS, Park K, Chae SS, Sboner A, MacDonald TY, et al. Molecular characterization of neuroendocrine prostate cancer and identification of new drug targets. Cancer Discov 2011;1:487–95.
5. Spiess PE, Pettaway CA, Vakar-Lopez F, Kassouf W, Wang X, Busby JE, et al. Treatment outcomes of small cell carcinoma of the prostate: a single-center study. Cancer 2007;110:1729–37.
6. Dardenne E, Beltran H, Benelli M, Gayvert K, Berger A, Puca L, et al. N-Myc Induces an EZH2-mediated transcriptional program driving neuroendocrine prostate cancer. Cancer Cell 2016;30:563–77.
7. Lee JK, Phillips JW, Smith BA, Park JW, Stoyanova T, McCaffrey EF, et al. N-Myc drives neuroendocrine prostate cancer initiated from human prostate epithelial cells. Cancer Cell 2016;29:536–47.
8. Bell E, Chen L, Liu T, Marshall GM, Lunec J, Tweddle DA. MYCN oncoprotein targets and their therapeutic potential. Cancer Lett 2010;293:144–57.
9. Beltran H. The N-myc oncogene: maximizing its targets, regulation, and therapeutic potential. Mol Cancer Res 2014;12:815–22.
10. Grasso CS, Wu YM, Robinson DR, Cao X, Dhanasekaran SM, Khan AP, et al. The mutational landscape of lethal castration-resistant prostate cancer. Nature 2012;487:239–43.
11. Mateo J, Carreira S, Sandhu S, Miranda S, Mossop H, Perez-Lopez R, et al. DNA-repair defects and olaparib in metastatic prostate cancer. N Engl J Med 2015;373:1697–708.
12. Simbulan-Rosenthal CM, Rosenthal DS, Luo R, Samara R, Espinoza LA, Hassa PO, et al. PARP-1 binds E2F-1 independently of its DNA binding and catalytic domains, and acts as a novel coactivator of E2F-1-mediated transcription during re-entry of quiescent cells into S phase. Oncogene 2003;22:8460–71.
13. Verlinden L, Vanden Bempt I, Eelen G, Drijkoningen M, Verlinden I, Marchal K, et al. The E2F-regulated gene Chk1 is highly expressed in triple-negative estrogen receptor/progesterone receptor/HER-2 breast carcinomas. Cancer Res 2007;67:6574–81.
14. Byers LA, Wang J, Nilsson MB, Fujimoto J, Saintigny P, Yordy J, et al. Proteomic profiling identifies dysregulated pathways in small cell lung cancer and novel therapeutic targets including PARP1. Cancer Discov 2012;2:798–811.
15. Hallett RM, Seong AB, Kaplan DR, Irwin MS. Transcript signatures that predict outcome and identify targetable pathways in MYCN-amplified neuroblastoma. Mol Oncol 2016;10:1461–72.
16. Wan X, Corn PG, Yang J, Palanisamy N, Starbuck MW, Efstathiou E, et al. Prostate cancer cell-stromal cell crosstalk via FGFR1 mediates antitumor activity of dovitinib in bone metastases. Sci Transl Med 2014;6:252ra122.
17. Roychowdhury S, Iyer MK, Robinson DR, Lonigro RJ, Wu YM, Cao X, et al. Personalized oncology through integrative high-throughput sequencing: a pilot study. Sci Transl Med 2011;3:111ra21.
18. Beltran H, Prandi D, Mosquera JM, Benelli M, Puca L, Cyrta J, et al. Divergent clonal evolution of castration-resistant neuroendocrine prostate cancer. Nat Med 2016;22:298–305.
19. Robinson D, Van Allen EM, Wu YM, Schultz N, Lonigro RJ, Mosquera JM, et al. Integrative clinical genomics of advanced prostate cancer. Cell 2015;161:1215–28.
20. Aparicio AM, Shen L, Tapia EL, Lu JF, Chen HC, Zhang J, et al. Combined tumor suppressor defects characterize clinically defined aggressive variant prostate cancers. Clin Cancer Res 2016;22:1520–30.
21. Tzelepi V, Zhang J, Lu JF, Kleb B, Wu G, Wan X, et al. Modeling a lethal prostate cancer variant with small-cell carcinoma features. Clin Cancer Res 2012;18:666–77.
22. Li L, Chang W, Yang G, Ren C, Park S, Karantanos T, et al. Targeting poly (ADP-ribose) polymerase and the c-Myb-regulated DNA damage response pathway in castration-resistant prostate cancer. Sci Signal 2014;7:ra47.
23. Li L, Karanika S, Yang G, Wang J, Park S, Broom BM, et al. Androgen receptor inhibitor-induced "BRCAness" and PARP inhibition are synthetically lethal for castration-resistant prostate cancer. Sci Signal 2017;10:pii: eaam7479.
24. Wu PY, Liao YF, Juan HF, Huang HC, Wang BJ, Lu YL, et al. Aryl hydrocarbon receptor downregulates MYCN expression and promotes cell differentiation of neuroblastoma. PLoS One 2014;9:e88795.
25. Otto T, Horn S, Brockmann M, Eilers U, Schuttrumpf L, Popov N, et al. Stabilization of N-Myc is a critical function of Aurora A in human neuroblastoma. Cancer Cell 2009;15:67–78.
26. Meulenbeld HJ, Bleuse JP, Vinci EM, Raymond E, Vitali G, Santoro A, et al. Randomized phase II study of danusertib in patients with metastatic castration-resistant prostate cancer after docetaxel failure. BJU Int 2013;111:44–52.
27. Hassa PO, Hottiger MO. The functional role of poly(ADP-ribose)polymerase 1 as novel coactivator of NF-kappaB in inflammatory disorders. Cell Mol Life Sci 2002;59:1534–53.
28. Kumar A, Coleman I, Morrissey C, Zhang X, True LD, Gulati R, et al. Substantial interindividual and limited intraindividual genomic diversity among tumors from men with metastatic prostate cancer. Nat Med 2016;22:369–78.